Debonding of a circular inclusion: Asymmetric propagation of a pair of cracks

Vinh Hoang Tan Le, Sébastien Brisard, Amade Pouya

Debonding of a circular inclusion: asymmetric propagation of a pair of cracks

Vinh Hoang Tan Le, Sébastien Brisard, Amade Pouya

This is the accepted version of the following article: “Debonding of a circular inclusion: asymmetric propagation of a pair of cracks”, which has been published in final form at https://doi.org/10.1016/j.ijsolstr.2019.03.004.

Debonding of a circular inclusion: asymmetric propagation of a pair of cracks

V.H.T. Le[a], S. Brisard[a,*], A. Pouya[a]

[a] *Université Paris-Est, Laboratoire Navier, UMR 8205, CNRS, ENPC, IFSTTAR, F-77455 Marne-la-Vallée, France*

Abstract

Crack propagation associated with two initially symmetrical cracks located at the interface between an inclusion and the surrounding matrix, subjected to remote traction, is studied by means of Griffith's energy criterion within the framework of Linear elastic fracture mechanics. Using Muskhelishvili's method of complex potentials, we derive semi-analytical expressions of the stress intensity factor and energy release rate at the crack-tip. Finally, the discussion of the crack propagation mode is investigated. Based on these results, we discuss the mode of propagation of the cracks. Our analysis points at the possibility of a single-sided, rather than simultaneous, symmetric crack growth, even if both initial configuration and loading are symmetric.

Keywords: Interfacial crack, Complex potentials, Stress intensity factor, Energy release rate, Griffith's energy criterion,

1. Introduction

A wide range of industrial materials as well as geomaterials fall into the category of matrix-inclusion composites. For such materials, debonding (interfacial cracking) is central to damage propagation and ultimate failure. From the perspective of modelling, it is therefore essential to be able to accurately describe the overall behavior of matrix-inclusion composites with partially cracked interfaces. The first step towards this goal is the analysis of interfacial cracks located at the boundary of a *single* inclusion, embedded in an infinite matrix.

Perlman and Sih (1967) and Toya (1974) have made significant contributions to the problem of a circular inclusion subjected to a uniform remote stress (plane, linear elasticity). These authors used the complex variable method of Muskhelishvili (1953) (see also Milne-Thomson, 1968) to derive closed-form solutions. More recently, Prasad and Simha (2002, 2003) used the same approach to analyze the case of a point load acting anywhere in the matrix. Similarly, Theotokoglou and Theotokoglou (2002) studied the case of a single interface crack and a non-uniform far field. They used the obtained solution to study the interaction between a curved interface crack and a straight bulk crack. This solution was later extended to a periodic array of fibers by Kushch et al. (2010). Finally, Hasebe et al. (1986); Hasebe and Yamamoto (2014, 2015) recently studied branching into the matrix. However, their approach, based on conformal mapping, seems to be significantly more involved than the approach of Perlman and Sih (1967).

Like fracture of homogeneous materials, fracture of bimaterials is governed by the asymptotic behavior of the stresses near the crack tip. Unlike homogeneous materials, though, the crack opening derived from a linear elastic analysis exhibits an oscillatory character near the crack tip, owing to the presence of a $r^{i\epsilon}$ factor [r: distance to the crack tip; ϵ: bimaterial constant of Williams (1959)]. These oscillations make the linear elastic solution unphysical, since they result in the interpenetration of the upper and lower crack faces near the crack tip (Sun and Jin, 2012). However, as argued by e.g. Rice (1988), the solution remains relevant for the purpose of analyzing crack propagation.

The state of stress at the tip of interfacial cracks combines both modes I and II, and the energy release rate G , combined with Irwin's formula (Irwin, 1957), which is known to extend to interfacial cracks (Malyshev and Salganik, 1965; Sun and Jih, 1987), was used to carry out this analysis.

The motivation for this work is the development of a micromechanical model for composites accounting for partially bounded inclusions and propagation of interfacial cracks. The basic building block for such a model is the fundamental solution to the problem of a single, partially bonded inclusion. In the case of uniaxial tension, hasty symmetry considerations would predict that two symmetrical cracks will develop (see figure 1 with $\beta_1 = \beta_2$). However, many studies suggest that, even under uniaxial tension, cracks may nucleate and propagate asymmetrically (Leguillon, 2002; Mantič, 2009; Kushch et al., 2011a; García et al., 2015).

The present work is therefore an investigation of the fundamental solution to the problem of two coaxial arc cracks of differing lengths around the interface of a circular inclusion, embedded in a homogeneous matrix and subjected to a remote stress. Within the framework of the Muskhelisvili complex potentials, we thus extend two special cases already studied in the literature: indeed, taking first $\beta_2 = 0$, then $\beta_1 = \beta_2$ (see figure 1), we retrieve the solutions of Perlman and Sih (1967); Toya (1974); Prasad and Simha (2003) for a single crack and of Prasad and Simha (2002) for two cracks that have the same length. Propagation of the crack(s) is then analyzed by means of energetic arguments.

The paper is organised as follows. In section 2, we briefly

*Corresponding author.

Email addresses: vinh-hoang-tan.le@enpc.fr (V.H.T. Le), sebastien.brisard@ifsttar.fr (S. Brisard), amade.pouya@enpc.fr (A. Pouya)

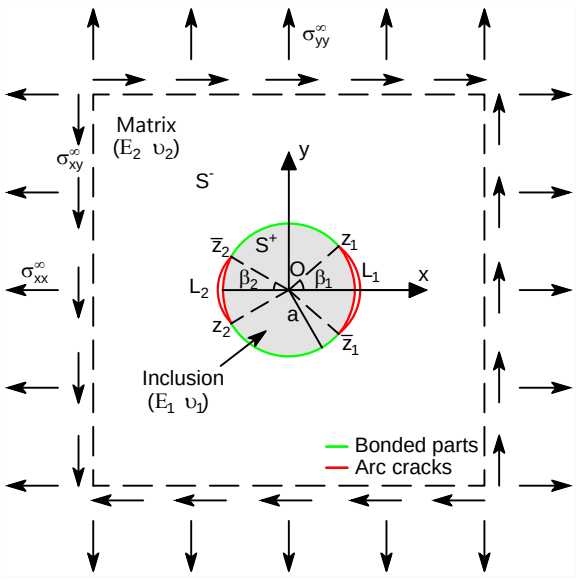

Figure 1: Two asymmetrical cracks at the inclusion-matrix interface under uniform stress at infinity

overview the derivation of our fundamental solution. In section 3, we deduce from this solution the complex stress intensity factors at the crack tip along an inclusion-matrix interface and the total energy release rate. The resulting semi-analytical expressions are compared with direct numerical simulation by the finite element method and the displacement extrapolation method (Ryoji and Sang-Bong, 1989; Gager, 2010). As an application, using energy-based arguments, section 4 finally discusses the symmetric vs. asymmetric propagation of two initially symmetric interfacial cracks.

2. Formulation and solution of problem

We consider the problem of a circular inclusion (radius: a) embedded in an infinite matrix, and subjected to a uniform stress at infinity. The matrix-inclusion interface is cracked along arcs L_1 and L_2. Both cracks are symmetrical about the horizontal axis; the arc cracks L_i ($i = 1, 2$) subtend an angle $2\beta_i$ (see figure 1). The Young modulus and Poisson ratio of the inclusion (resp. the matrix) are denoted E_1 and ν_1 (resp. E_2 and ν_2). Finally, it will be convenient to introduce the domains S^+ (resp. S^-) occupied by the inclusion (resp. the matrix).

The remainder of this section is devoted to the derivation of the solution to this problem. Following Prasad and Simha (2002) who studied the case of two identical cracks, we use the method of complex potential functions (Muskhelishvili, 1953; Milne-Thomson, 1968).

Before we proceed with the derivation, it should be noted that symmetry about the horizontal axis is not necessary. The general solution of Perlman and Sih (1967) applies even to unsymmetric cases. However the symmetry assumption allows us to go farther than these general solutions and to derive semi-analytical expressions of the stress intensity factors. These solutions are crucial for the discussion of stability.

2.1. General form of the solution

Following the notation of Milne-Thomson (1968), the displacement $\mathbf{u}$ and stress $\boldsymbol{\sigma}$ are expressed in terms of the complex functions W and w as follows

$$(\sigma_{rr})_j + (\sigma_{r\theta})_j = W_j(z) + \overline{W}_j(\overline{z}), \tag{1}$$

$$2[(\sigma_{rr})_j + \mathrm{i}(\sigma_{r\theta})_j] = W_j(z) + \overline{W}_j(\overline{z}) - \overline{z}\overline{W}'_j(\overline{z}) - (\overline{z}/z)\overline{w}_j(\overline{z}), \tag{2}$$

$$4\mu_j \frac{\partial}{\partial\theta}[(u_x)_j + \mathrm{i}(u_y)_j] = \mathrm{i}z[\kappa_j W_j(z) - \overline{W}_j(\overline{z}) + \overline{z}\overline{W}'_j(\overline{z}) + (\overline{z}/z)\overline{w}_j(\overline{z})], \tag{3}$$

where $j = 1$ for $z \in S^+$ (inclusion) and $j = 2$ for $z \in S^-$ (matrix) and

$$\kappa_{j,\text{ plane stress}} = \frac{3-\nu_j}{1+\nu_j} \quad \text{and} \quad \kappa_{j,\text{ plane strain}} = 3 - 4\nu_j. \tag{4}$$

We will also use the following bi-material constants

$$\alpha = \frac{\mu_1 + \kappa_1\mu_2}{\mu_2 + \kappa_2\mu_1}, \quad m = \frac{\mu_1(1+\kappa_2)}{\mu_2(1+\kappa_1)} \quad \text{and} \quad \epsilon = \frac{\ln\alpha}{2\pi}, \tag{5}$$

where $\mu_i = E_i/[2(1+\nu_i)]$, $i = 1, 2$ denotes the shear modulus, E_i denotes the Young modulus and ν_i denotes the Poisson ratio; ϵ is known as the oscillatory index.

For circular cracks, it is convenient to introduce the functions Ω_j defined as follows (Perlman and Sih, 1967; Prasad and Simha, 2002)

$$\Omega_j(z) = -\overline{W}_j\left(\frac{a^2}{z}\right) + \frac{a^2}{z}\overline{W}'_j\left(\frac{a^2}{z}\right) + \frac{a^2}{z^2}\overline{w}_j\left(\frac{a^2}{z}\right). \tag{6}$$

Perlman and Sih (1967) derived the general expression of W_1, W_2, Ω_1 and Ω_2 for a set of n circular cracks. Following the notation of Prasad and Simha (2002), these expressions read, for $n = 2$

$$(1+\alpha)W_1(z) = mQ(z) + \chi(z)P(z), \tag{7}$$

$$(1+\alpha)\Omega_1(z) = mQ(z) - \alpha\chi(z)P(z), \tag{8}$$

$$(1+\alpha)W_2(z) = Q(z) + \alpha\chi(z)P(z), \tag{9}$$

$$(1+\alpha)\Omega_2(z) = Q(z) - \chi(z)P(z), \tag{10}$$

where we have introduced the Plemelj function ($z_1 = a\mathrm{e}^{\mathrm{i}\beta_1}$, $z_2 = a\mathrm{e}^{\mathrm{i}(\beta_2-\pi)}$)

$$\chi(z) = (z-\overline{z_1})^{-\frac{1}{2}+\mathrm{i}\epsilon}(z-z_1)^{-\frac{1}{2}-\mathrm{i}\epsilon}(z-\overline{z_2})^{-\frac{1}{2}+\mathrm{i}\epsilon}(z-z_2)^{-\frac{1}{2}-\mathrm{i}\epsilon}, \tag{11}$$

and

$$Q(z) = e_0 + \frac{t_1}{z} + \frac{t_2}{z^2}, \quad P(z) = P_2z^2 + P_1z + P_0 + \frac{P_{-1}}{z} + \frac{P_{-2}}{z^2}, \tag{12}$$

e_0, t_1, t_2, $P_{-2}, \ldots, P_2$ being 8 constants to be determined. This is discussed in the next section.

2.2. Determination of the integration constants

The 8 integration constants introduced above are found from: *i.* the behavior at infinity of W_2 and w_2 (4 equations), *ii.* the analyticity of W_1 and w_1 at $z = 0$ (3 equations) and *iii.* the single-valuedness of the displacements (1 equation). These three items are briefly described below.

Behavior at infinity of W_2 and w_2. From Milne-Thomson (1968, chap. IV, §4.10), these functions behave as follows

$$W_2(z) = A^\infty + O(z^{-2}) \qquad (z \to \infty), \tag{13}$$
$$w_2(z) = B^\infty + O(z^{-2}) \qquad (z \to \infty), \tag{14}$$

where

$$2A^\infty = \sigma^\infty_{xx} + \sigma^\infty_{yy} \quad \text{and} \quad B^\infty = \sigma^\infty_{yy} - \sigma^\infty_{xx} + 2\mathrm{i}\sigma^\infty_{xy}, \tag{15}$$

and $\boldsymbol{\sigma}^\infty$ denotes the remote stress.

In the present section, we will make use of the asymptotic expansions of the Plemelj function χ at infinity and about the origin

$$\chi(z) = z^{-2}[1 + z^{-1}F_{21} + O(z^{-2})] \qquad (z \to \infty), \tag{16}$$
$$\chi(z) = F_{10}(1 + zF_{11} + z^2F_{12}) + O(z^3) \qquad (z \to 0), \tag{17}$$

where the symbols F_{ij} were introduced by Prasad and Simha (2002) for $\beta_1 = \beta_2$. For $\beta_1 \neq \beta_2$, we find

$$a^2F_{10} = -\exp[2\epsilon(\beta_1 + \beta_2)], \tag{18}$$
$$aF_{11} = \cos\beta_1 - \cos\beta_2 + 2\epsilon(\sin\beta_1 - \sin\beta_2), \tag{19}$$
$$\begin{aligned} a^2F_{12} = {} & \epsilon^2(2 - \cos 2\beta_1 - \cos 2\beta_2 - 4\sin\beta_1\sin\beta_2) \\ & + 2\epsilon[\sin 2\beta_1 + \sin 2\beta_2 - \sin(\beta_1 + \beta_2)] \\ & + \tfrac{1}{2} + \tfrac{3}{4}(\cos 2\beta_1 + \cos 2\beta_2) - \cos\beta_1\cos\beta_2, \end{aligned} \tag{20}$$
$$a^{-1}F_{21} = \cos\beta_1 - \cos\beta_2 - 2\epsilon(\sin\beta_1 - \sin\beta_2). \tag{21}$$

Plugging expansion (16) into equation (9) and identifying with equation (13), we find

$$\alpha P_2 + e_0 = (1 + \alpha)A^\infty \quad \text{and} \quad \alpha P_1 + \alpha F_{21}P_2 + t_1 = 0. \tag{22}$$

Then, combining equations (6), (13) and (14) delivers the following expansion of Ω_2 at $z = 0$

$$\Omega_2(z) = \frac{a^2}{z^2}\overline{B^\infty} + O(1) \qquad (z \to 0), \tag{23}$$

which upon identification with equation (10) leads to

$$-F_{10}P_{-2} + t_2 = (1 + \alpha)a^2\overline{B^\infty}, \tag{24}$$
$$F_{10}F_{11}P_{-2} + F_{10}P_{-1} - t_1 = 0. \tag{25}$$

Analyticity of W_1 and w_1 at $z = 0$. We finally express that both W_1 and w_1 must be analytic at $z = 0$. Expanding equation (7) and expressing that the negative power of z must vanish lead to

$$F_{10}P_{-2} + m\,t_2 = 0 \quad \text{and} \quad F_{10}F_{11}P_{-2} + F_{10}P_{-1} + m\,t_1 = 0. \tag{26}$$

To express the analyticity of w_1 at $z = 0$, we combine equations (6) with the asymptotic expansions of equations (7) and (8) at $z \to 0$ and $z \to \infty$, respectively. We get

$$F_{10}F_{12}P_{-2} + F_{10}(F_{11}P_{-1} + P_0) - \alpha\overline{P_2} + m(e_0 + \overline{e_0}) = 0, \tag{27}$$

and

$$\alpha P_1 + \alpha F_{21}P_2 - m\,t_1 = 0. \tag{28}$$

Equations (22), (24), (25), (26) and (28) then lead to

$$e_0 = (1 + \alpha)A^\infty - \alpha P_2, \quad t_1 = 0, \quad t_2 = \frac{1 + \alpha}{1 + m}a^2\overline{B^\infty}, \tag{29}$$
$$P_{-2} = -\frac{m}{F_{10}}t_2, \quad P_{-1} = \frac{m\,F_{11}}{F_{10}}t_2, \quad P_1 = -F_{21}P_2, \tag{30}$$

and it is seen that there remains only two unknown integration constants, namely: P_0 and P_2, which are related through equation (27)

$$\begin{aligned} \alpha(1 + 2m)\Re(P_2) - \mathrm{i}\alpha\Im(P_2) - F_{10}P_0 = m\frac{1 + \alpha}{1 + m}[2(1 + m)A^\infty \\ + (F_{11}^2 - F_{12})a^2\overline{B^\infty}], \end{aligned} \tag{31}$$

where $\Re$ and $\Im$ denote the real and imaginary parts of their argument.

Single-valuedness of the displacements. The remaining equation is found from the condition of single-valuedness of the displacements (Perlman and Sih, 1967)

$$\int_{L_j} \chi^+(t)(P_2t^2 + P_1t + P_0 + P_{-1}t^{-1} + P_{-2}t^{-2})\mathrm{d}t = 0, \tag{32}$$

where it is recalled that L_j ($j = 1, 2$) denotes one of the two arc cracks, while χ^+ is defined on $L_1 \cup L_2$ as follows

$$\chi^+(a\mathrm{e}^{\mathrm{i}\theta}) = \lim_{r \overset{<}{\to} a-} \chi^+(r\mathrm{e}^{\mathrm{i}\theta}). \tag{33}$$

Selecting crack L_1 (located between $z = a\mathrm{e}^{-\mathrm{i}\beta_1}$ and $z = a\mathrm{e}^{\mathrm{i}\beta_1}$) in equation (32), we get the condition

$$I_2P_2 + I_1P_1 + I_0P_0 + I_{-1}P_{-1} + I_{-2}P_{-2} = 0, \tag{34}$$

where

$$I_k = a^k\int_{-\beta_1}^{\beta_1} \frac{\cos[\epsilon\ln f_1(\beta_1, \beta_2, \theta) - k\theta]}{\sqrt{f_2(\beta_1, \beta_2, \theta)}}\mathrm{d}\theta, \tag{35}$$

for $k = -2, -1, 0, 1, 2$, with

$$f_1(\beta_1, \beta_2, \theta) = g_1(\beta_1, \beta_2, \theta)/g_2(\beta_1, \beta_2, \theta), \tag{36}$$
$$f_2(\beta_1, \beta_2, \theta) = g_1(\beta_1, \beta_2, \theta)\,g_2(\beta_1, \beta_2, \theta), \tag{37}$$
$$g_1(\beta_1, \beta_2, \theta) = \sin\tfrac{1}{2}(\beta_1 - \theta)\cos\tfrac{1}{2}(\beta_2 - \theta) \tag{38}$$
$$g_2(\beta_1, \beta_2, \theta) = \sin\tfrac{1}{2}(\beta_1 + \theta)\cos\tfrac{1}{2}(\beta_2 + \theta). \tag{39}$$

Integrals (35) are singular; indeed, when $\theta \to \beta_1$, the argument of the logarithm tends to 0, and the numerator of the integrand oscillates at a frequency that grows exponentially. In order to minimize round-off errors, numerical evaluation of these integrals should normally require that: *i.* the contribution of each oscillation be computed and stored, *ii.* positive and negative contributions (ordered by increasing magnitude) be summed separately, *iii.* the sum of all positive contributions be added to the sum of all negative contributions. Finally, it should be noted that a rigorous bound on the numerical error

can be produced by means of standard results on alternating series.

However, in the present case, the contribution of each new oscillation decreases exponentially, to the point that even the *first* oscillation vanishes up to machine precision. The above described rigorous approach therefore turned out to be unnecessary, and we relied without further precautions on the standard `quad` function from the `scipy.integrate` Python package[1] (wich is a wrapper around the Fortran `QUADPACK` library) to compute the integrals I_k.

Expression of P_2. Solving equations (31) and (34) finally leads to

$$\begin{aligned}\Re(P_2) = \{&F_{10}[(F_{12}I_0 - I_{-2})\Re(P_{-2}) + (F_{11}I_0 - I_{-1})\Re(P_{-1})] \\ &+ 2m(1+\alpha)I_0A^\infty\}(2\alpha m I_0 - F_{10}F_{21}I_1 + \alpha I_0 \\ &+ F_{10}I_2)^{-1} \qquad (40)\\ \Im(P_2) = &-F_{10}[(F_{12}I_0 - I_{-2})\Im(P_{-2}) + (F_{11}I_0 - I_{-1})\Im(P_{-1})] \\ &\cdot (F_{10}F_{21}I_1 + \alpha I_0 - F_{10}I_2)^{-1}, \qquad (41)\end{aligned}$$

and P_0 is then deduced from e.g. equation (34).

In the next section, the above results are used to express the stress intensity factors, from which the total energy release rate is then deduced. The latter is eventually used in section 4 to analyse the crack propagation.

3. Stress intensity factors and energy release rate

3.1. Complex stress intensity factor

The analytical solution for a plane interface crack between two elastic isotropic materials was obtained by Williams (1959) who found the stresses along the bonded part of the interface and the relative displacements of two lips of the crack, $\Delta u_i(s) = u_i(s, \varphi = \pi) - u_i(s, \varphi = -\pi)$. According to this solution, the asymptotic expression for the stress and relative displacement when $s \to 0$ (s is the distance from the tip) is the following:

$$\sigma_{nn}(s, \varphi = 0) + \mathrm{i}\sigma_{nt}(s, \varphi = 0) = \frac{\mathcal{K}}{\sqrt{2\pi}} s^{\mathrm{i}\epsilon - 1/2}, \qquad (42)$$

$$\Delta u_n(s) + \mathrm{i}\Delta u_t(s) = \frac{8}{(1+2\mathrm{i}\epsilon)\cosh(\pi\epsilon)E^*} \frac{\mathcal{K}}{\sqrt{2\pi}} s^{\mathrm{i}\epsilon + 1/2}, \qquad (43)$$

where s and φ are the polar coordinates with pole at the crack-tip (see Figure 2, left) and $2/E^* = 1/E_1^* + 1/E_2^*$ ($E_j^* = E_j$ for plane stress problems, $E_j^* = E_j/(1-\nu_j^2)$ for plane strain problems).

In the above expressions, $\mathcal{K}$ denotes the complex stress intensity factor, with "awkwardly complex" (Rice, 1988) physical dimensions: MPa $\cdot$ m$^{1/2-\mathrm{i}\epsilon}$. It is customary to define stress intensity factors K_I and K_II in the classical sense (with physical dimensions: MPa $\cdot$ $\sqrt{\mathrm{m}}$) through the introduction of an additional reference length ℓ (Rice, 1988)

$$K_\mathrm{I} + \mathrm{i}K_\mathrm{II} = \ell^{\mathrm{i}\epsilon}\mathcal{K}. \qquad (44)$$

Selecting an appropriate value for the reference length ℓ is in general a difficult task, for which there is no clear methodology. However, for the present study, ℓ can be chosen arbitrarily. Indeed, in section 3.3, we compare analytical values of K_I and K_II with finite element estimates; for the purpose of this comparison, ℓ should merely be seen as a normalization constant. Then, in sections 3.4 and 4, our analysis of the propagation of cracks is based on the energy release rate G and the interfacial thoughness G_c. Neither the energy release rate [see equation (53)], nor the interfacial toughness (which is assumed constant) depend on ℓ. We therefore chose arbitrarily $\ell = a$ in the remainder of this paper.

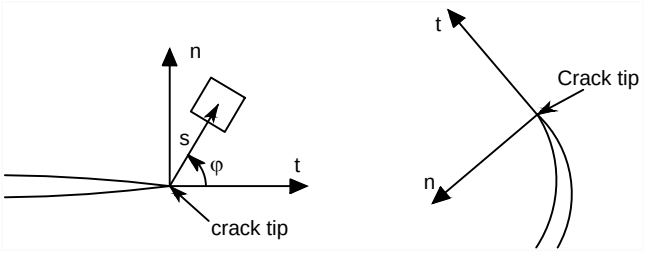

Figure 2: The local coordinate system (n, t) at the crack tip

The asymptotic expansions (42) and (43) hold for curved cracks as well. In the present case, σ_{nn} and σ_{nt} can be related to σ_{rr} and $\sigma_{r\theta}$ as follows (see Figure 2, right)

$$\sigma_{nn} + \mathrm{i}\sigma_{nt} = \sigma_{rr} - \mathrm{i}\sigma_{r\theta}. \qquad (45)$$

From equations (2) and (6), the traction on the bonded part of the interface can be expressed as

$$2[(\sigma_{rr})_1 + \mathrm{i}(\sigma_{r\theta})_1](a\mathrm{e}^{\mathrm{i}\theta}) = W_1^+(a\mathrm{e}^{\mathrm{i}\theta}) - \Omega_1^-(a\mathrm{e}^{\mathrm{i}\theta}), \qquad (46)$$

where $\beta_1 < \theta < \pi - \beta_2$ (or $-\pi + \beta_2 < \theta < -\beta_1$). Furthermore, superscripts $+$ and $-$ in functions W_1 and Ω_1 denote the limit values when $z \to a\mathrm{e}^{\mathrm{i}\theta}$ from $z \in S^+$ (inclusion) and $z \in S^-$ (matrix), respectively.

Substituting in equation (46) the expressions (7) and (8) of the complex potentials W_1 and Ω_1 and using the continuity of P, Q and χ (in the bonded part of the interface) delivers

$$\sigma_{rr} + \mathrm{i}\sigma_{r\theta} = \tfrac{1}{2}\chi(a\mathrm{e}^{\mathrm{i}\theta})P(a\mathrm{e}^{\mathrm{i}\theta}). \qquad (47)$$

Then the complex stress intensity factor $\mathcal{K}$ at the crack tip $z_1 = a\mathrm{e}^{\mathrm{i}\beta_1}$ is obtained from an asymptotic expansion of $\chi(a\mathrm{e}^{\mathrm{i}\theta})$, for $\theta \xrightarrow{>} \beta_1$:

$$\begin{aligned}\overline{a^{\mathrm{i}\epsilon}\mathcal{K}} &= K_\mathrm{I} - \mathrm{i}K_\mathrm{II} \\ &= \frac{-\mathrm{i}\sqrt{2\pi}\,\exp[\epsilon(\beta_1+\beta_2) - \mathrm{i}(\epsilon\psi + \beta_1)]P(a\mathrm{e}^{\mathrm{i}\beta_1})}{4a\sqrt{2a\sin\beta_1\cos\tfrac{1}{2}(\beta_1+\beta_2)\cos\tfrac{1}{2}(\beta_1-\beta_2)}}, \qquad (48a)\end{aligned}$$

[1] https://docs.scipy.org/doc/scipy/reference/tutorial/integrate.html, last retrieved 2019-01-24.

where

$$\psi = \ln \frac{\cos \frac{1}{2}(\beta_1 - \beta_2)}{2 \sin\beta_1 \cos \frac{1}{2}(\beta_1 + \beta_2)}. \tag{48b}$$

It is readily verified that the results of Prasad and Simha (2003) (single crack) and Prasad and Simha (2002) (two identical cracks) are retrieved from equation (48), if we let $\beta_2 = 0$ or $\beta_2 = \beta_1 = \beta$, respectively.

3.2. Validity of the solution

Owing to the $s^{i\epsilon}$ factor in equation (43), the displacements of the crack surfaces exhibit an oscillatory character, leading to the upper and lower crack surfaces to overlap near the crack tip. This is physically unrealistic, and the linear elastic solution presented above should be replaced with a non-linear solution accounting for contact. However, as argued by Rice (1988), the linear elastic solution delivers an acceptable approximation of the true solution if the size of the contact area remains small compared with the total crack length.

Let s_c be the size of the contact zone; it is the largest value of s such that $\Delta u_n(s) = 0$ and

$$s_c \leq 2a\beta_1 \tag{49}$$

(the contact zone must be shorter than the crack). It can readily be found that s_c maximizes under the constraint (49) the following quantity (Sun and Qian, 1997)

$$s_c = \exp\left[\frac{1}{\epsilon}\left\{\tan^{-1}\left(\frac{\Re(\mathcal{K}) + 2\epsilon\Im(\mathcal{K})}{\Im(\mathcal{K}) - 2\epsilon\Re(\mathcal{K})}\right) + n\pi\right\}\right], \tag{50}$$

for $n = \ldots, -2, -1, 0, 1, 2, \ldots$. The above expression does not depend on the reference length ℓ, as emphasized by the fact that we used the complex stress-intensity factor $\mathcal{K}$ to express this value rather than K_I and K_{II}.

In the case of a hard inclusion subjected to a uniaxial remote stress along the x-axis, we have plotted s_c in Figure 3 for various values of β_1 and β_2 (for each curve, β_2 is fixed, while β_1 varies). This figure clearly shows that the extent of the contact zone remains negligible for values of β_1 up to about 55°. As a consequence, it will always be assumed in the remainder of this paper that the cracks are such that $\beta_1, \beta_2 \leq 55°$, so that the linear elastic solution derived above is an excellent approximation to the true (non-linear) solution.

3.3. Comparison with a finite element analysis

We performed a finite element analysis of the above problem with various configurations of the two cracks to check the consistency of our analytical results. We used the finite element code `Porofis` (Pouya, 2015) to perform plane strains simulations.

The model is depicted on figure 4. In order to minimize boundary effects, we selected a large domain size $H = 40a$. Uniaxial tractions $\sigma_{xx} = \sigma^{\infty}_{xx}$ are applied to the left and right edges of this domain while the upper and lower edges are stress-free. We used three-node, linear elements and compensated for

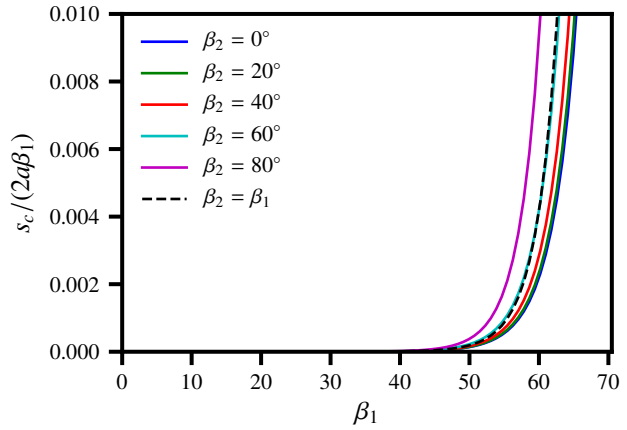

Figure 3: Size of the contact zone s_c for a hard inclusion subjected to a uniaxial remote stress along the x-axis.

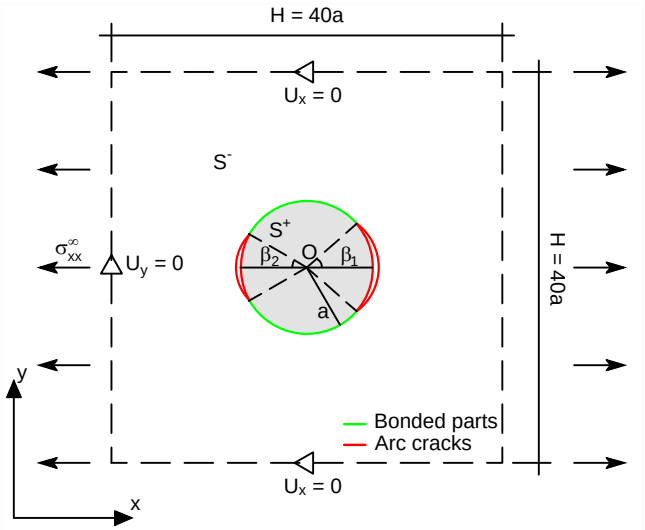

Figure 4: Geometry of the numerical simulations described in section 3.3.

their low accuracy (quadratic elements would have been better-suited) with a fine mesh (mesh size $\sim 0.001a$ near the boundary, away from the crack-tips; mesh size $\simeq 10^{-5}a$ near the crack-tips).Various crack geometries were considered (each resulting in a different mesh):

1. a single crack, i.e $\beta_2 = 0$ and $\beta_1 = 5°, 10°, 15°, \ldots, 55°$,
2. two symmetrical cracks, i.e $\beta_1 = \beta_2 = 5°, 10°, 15°, \ldots, 55°$,
3. two asymmetrical cracks: $\beta_2 = 30°$ and $\beta_1 = 5°, 10°, 15°, \ldots, 55°$,

and figure 5 shows the mesh that was used for $\beta_1 = 40°$ and $\beta_2 = 30°$. For each geometry, the stress intensity factors are estimated for the various combinations of material properties

1. $E_1 = E_2$ and $\nu_1 = \nu_2 = 0.25$ (homogeneous case),
2. $E_1 = 10E_2$, $\nu_1 = 0.2$ and $\nu_2 = 0.3$ (hard inclusion),
3. $E_2 = 10E_1$, $\nu_1 = 0.2$ and $\nu_2 = 0.3$ (soft inclusion).

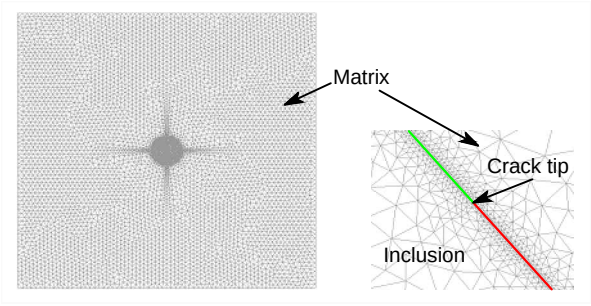

Figure 5: Example of triangular mesh that was generated for the asymmetric case $\beta_1 = 40°$ and $\beta_2 = 30°$.

We estimated the stress intensity factors K_I and K_II from the quantities $Q_\mathrm{I}(s)$ and $Q_\mathrm{II}(s)$ defined as follows [see equation (43)]:

$$Q_\mathrm{I} + \mathrm{i}Q_\mathrm{II} = \frac{1+2\mathrm{i}\epsilon}{8}\sqrt{2\pi}E^*\cosh(\pi\epsilon)\left(\frac{a}{s}\right)^{\mathrm{i}\epsilon}(\Delta u_n + \mathrm{i}\Delta u_t), \qquad (51)$$

where $\Delta u_n(s)$ and $\Delta u_t(s)$ denote the normal and tangent components of the displacement discontinuity (s: arc-length from crack tip), which are outputs of the numerical code. As $s \to 0$, this quantity should behave as

$$Q_\mathrm{I} + \mathrm{i}Q_\mathrm{II} \sim (K_\mathrm{I} + \mathrm{i}K_\mathrm{II})\sqrt{s}, \quad s \to 0. \qquad (52)$$

Figure 6 plots nodal values of Q_I and Q_II as a function of $\sqrt{s}$. As expected, both quantities vary quasi-linearly with $\sqrt{s}$, which allows to compute K_I and K_II through linear regression. To do so, we selected nodes that are both not too close to the crack-tip (where the quality of the fit deteriorates, owing to the singularity) and not too far from the crack-tip [where the asymptotic behavior (52) no longer holds]. We found that the range $0.03 \le \sqrt{s/a} \le 0.06$ resulted in a satisfactory fit for all cases considered here.

Figures 7 and 8 show good agreement between the stress intensity factors thus estimated and the analytical formula (48) for $\beta_2 = 30°$ and the whole range of β_1-values listed above. More extensive comparison (not shown here) confirms that this good agreement carries through the whole range of β_2-values.

3.4. Total energy release rate

Following Sun and Jin (2012), we consider a crack propagation criterion based on the energy release rate. The total energy release rate of a bimaterial interface crack can be related to the complex stress intensity factor through the following extension of Irwin's formula (Malyshev and Salganik, 1965):

$$G = \frac{1}{E^*}\frac{\mathcal{K}\overline{\mathcal{K}}}{\cosh^2(\pi\epsilon)}. \qquad (53)$$

Figure 9 plots, for a hard inclusion under uniaxial far field stress σ^∞_{xx}, the total energy release rate at the crack-tip $z_1 = \mathrm{e}^{\mathrm{i}\beta_1}$. For each solid curve in this figure, β_2 is fixed, while β_1 varies from 0° to 60°. The broken line refers to the energy release rate for the symmetric case $\beta_1 = \beta_2$.

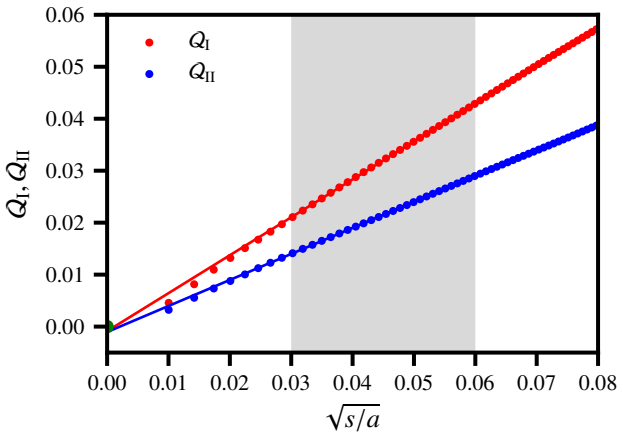

Figure 6: Linear regression of the numerical quantities Q_I and Q_II, which should behave linearly w.r.t $\sqrt{s}$. The quality of the fit deteriorates for nodes that are too close or too far from the crack-tip. Therefore, only the nodes located in the shaded area are used to perform the linear regression. (hard inclusion, $\beta_1 = 40°, \beta_2 = 30°$)

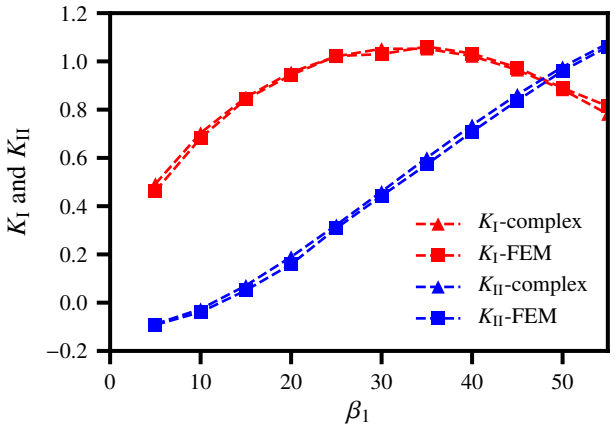

Figure 7: K_I and K_II vs. β_1 (two asymmetrical cracks, $\beta_2 = 30°$, hard inclusion).

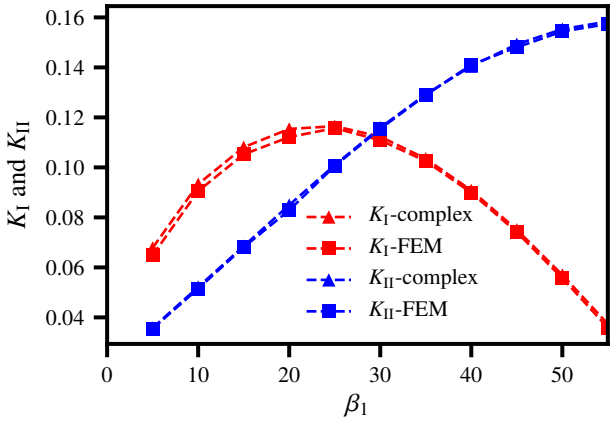

Figure 8: K_I and K_II vs. β_1 (two asymmetrical cracks, $\beta_2 = 30°$, soft inclusion).

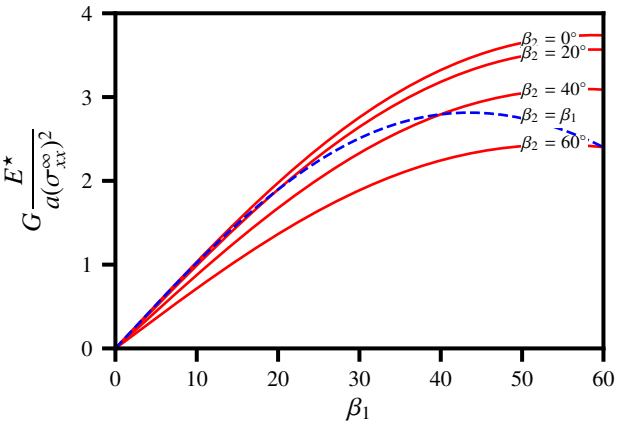

Figure 9: Normalized energy release rate (hard inclusion, uniaxial stress at infinity).

The plot $\beta_2 = 0°$ represents the classical results of Toya (1974) (single crack). Observation of figure 9 shows that the energy release rate is a decreasing function of β_2 (β_1 being fixed). This can be explained by the fact that, for the same far field stress, a greater value of β_2 decreases the stress intensities at z_1. Note that the same trends are observed for the homogeneous and the soft inclusion cases (figures not reproduced here).

4. Discussion: symmetric versus asymmetric propagation

In this section, we provide a simple application that illustrates how the above analytical results can be used. We consider a partially bonded circular inclusion, as depicted in Figure 1, with $\beta_1 = \beta_2 = \beta_0$ (*symmetric* initial configuration). It is emphasized that we do not assume that debonding from $\beta_1 = \beta_2 = 0$ to $\beta_1 = \beta_2 = \beta_0 > 0$ occured through a crack nucleation/propagation process. Rather, we assume that the sample was *created* with a partially bonded interface and therefore discard any discussion regarding stable vs. unstable propagation of the cracks from $\beta_i = 0$ to $\beta_i = \beta_0$. However contrived, this example lends itself to an interesting analysis, namely the discussion of symmetric versus asymmetric crack propagation.

More precisely, the inclusion is subjected to a uniaxial remote tension σ_{xx}^∞ in the x-direction (Figure 10). When the loading reaches a critical value, cracks 1 and 2 start to propagate. Introducing the increments $\delta\beta_1$ and $\delta\beta_2$ of the crack angles, hasty symmetry considerations suggest that $\delta\beta_1 = \delta\beta_2$. The analysis proposed below shows that in fact, the situation may be more complex, with two possible outcomes: *i.* symmetric propagation ($\delta\beta_1 = \delta\beta_2 > 0$) and asymmetric propagation ($\delta\beta_1 > 0$ and $\delta\beta_2 = 0$, or $\delta\beta_2 > 0$ and $\delta\beta_1 = 0$) where only one crack propagates. Note that these results are supported (and in fact, motivated) by finite element simulations (not shown here) using a cohesive zone model.

Our discussion is based on energetic arguments, under the following assumptions:

1. The selected propagation mode minimizes the total energy for a prescribed total crack length creation, as argued by e.g. Griffith (1921); Erdogan and Sih (1963).

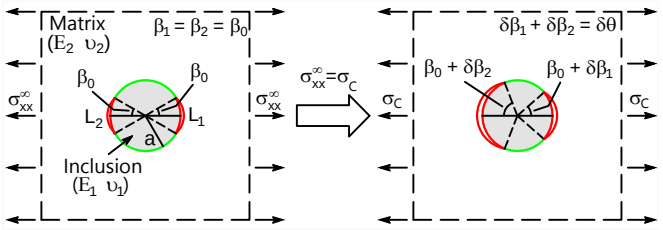

Figure 10: Discussion of the crack growth mode (σ_C denotes the critical value of the stress at infinity that results in propagation).

2. Branching of the cracks into the matrix or the inclusion is not considered.
3. Both cracks propagate symmetrically with respect to the x-axis.
4. The critical value G_c is assumed constant.

It should be noted that Assumption 3 is a rather strong assumption for which we have no theoretical justification. However, our numerical simulations seem to confirm that symmetry will first be broken about the y-axis, rather than the x-axis, as we intuitively thought.

The total energy Π of the system, to be minimized according to assumption 1, is the sum of the potential energy W_p and the dissipated energy W_s. Owing to assumption 4, we have $W_s(\beta_1,\beta_2) = 2a\,(\beta_1+\beta_2)\,G_c$, and

$$\Pi(\beta_1,\beta_2) = W_p(\beta_1,\beta_2) + 2a\,(\beta_1+\beta_2)\,G_c. \tag{54}$$

Starting from an initial configuration (β_1,β_2), propagation will occur if a nearby configuration $(\beta_1+\delta\beta_1,\beta_2+\delta\beta_2)$ such that $\Pi(\beta_1+\delta\beta_1,\beta_2+\delta\beta_2) < \Pi(\beta_1,\beta_2)$ can be exhibited with $\delta\beta_i \geq 0$ $(i = 1,2)$. Since we explore only nearby states, the energy Π can be expanded about the initial state (β_1,β_2):

$$\begin{aligned}\Pi(\beta_1+\delta\beta_1,\beta_2+\delta\beta_2) \simeq\ & \frac{\partial W_p}{\partial\beta_1}\delta\beta_1 + \frac{\partial W_p}{\partial\beta_2}\delta\beta_2 + 2a(\delta\beta_1+\delta\beta_2)G_c \\ & + \frac{\partial^2 W_p}{\partial\beta_1^2}\frac{\delta\beta_1^2}{2} + \frac{\partial^2 W_p}{\partial\beta_1\partial\beta_2}\delta\beta_1\delta\beta_2 + \frac{\partial^2 W_p}{\partial\beta_2^2}\frac{\delta\beta_2^2}{2},\end{aligned} \tag{55}$$

where the derivatives of W_p are evaluated at β_1,β_2. Introducing the energy release rate $G_i(\beta_1,\beta_2)$, $(i = 1,2)$ at the tips of crack L_i, we have the classical relation

$$G_i(\beta_1,\beta_2) = -\frac{1}{2a}\frac{\partial W_p}{\partial\beta_i}, \tag{56}$$

where assumption 3 has been used (which accounts for the factor 2 in the above equation). Combining equations (55) and (56), we find

$$\begin{aligned}\Pi(\beta_1+\delta\beta_1,\beta_2+\delta\beta_2) \simeq\ & \Pi(\beta_1,\beta_2) \\ & + 2a(G_c - G_1)\delta\beta_1 + 2a(G_c - G_2)\delta\beta_2 \\ & - a\frac{\partial G_1}{\partial\beta_1}\delta\beta_1^2 - 2a\frac{\partial G_1}{\partial\beta_2}\delta\beta_1\delta\beta_2 - a\frac{\partial G_2}{\partial\beta_2}\delta\beta_2^2,\end{aligned} \tag{57}$$

which shows that propagation can occur only if $G_1 = G_c$ or $G_2 = G_c$. In the present case, $\beta_1 = \beta_2 = \beta_0$, which means that

$$G_1 = G_2 = G_c \quad \text{and} \quad \frac{\partial G_1}{\partial\beta_1} = \frac{\partial G_2}{\partial\beta_2} \qquad (\beta_1 = \beta_2 = \beta_0) \tag{58}$$

at the onset of propagation. Plugging into equation (57), we then have

$$\Pi(\beta_0+\delta\beta_1,\beta_0+\delta\beta_2) \simeq \Pi(\beta_0,\beta_0) - a(\delta\beta_1^2+\delta\beta_2^2)\left.\frac{\partial G_1}{\partial\beta_1}\right|_{\beta_1=\beta_2=\beta_0} - 2a\delta\beta_1\delta\beta_2\left.\frac{\partial G_1}{\partial\beta_2}\right|_{\beta_1=\beta_2=\beta_0}. \tag{59}$$

According to assumption 1, the propagation mode is such that the energy decrease is maximized, the total length of cracks created being prescribed. In other words, if the total propagation length $\delta\theta$ is considered, we consider propagation modes of the form

$$\delta\beta_1 = \lambda\delta\theta,\ \delta\beta_2 = (1-\lambda)\,\delta\theta, \tag{60}$$

where $0 \le \lambda \le 1$, and minimize $\Pi(\beta_0+\lambda\delta\theta,\beta_0+(1-\lambda)\,\delta\theta)$ with respect to λ. From equations (59) and (60),

$$\Pi(\beta_0+\lambda\delta\theta,\beta_0+(1-\lambda)\,\delta\theta) \simeq \Pi(\beta_0,\beta_0) - a\delta\theta^2\left.\frac{\partial G_1}{\partial\beta_1}\right|_{\beta_1=\beta_2=\beta_0} + 2a\lambda(1-\lambda)\Psi(\beta_0)\delta\theta^2, \tag{61}$$

$$\text{where}\quad \Psi(\beta_0) = \left.\frac{\partial G_1}{\partial\beta_1}\right|_{\beta_1=\beta_2=\beta_0} - \left.\frac{\partial G_1}{\partial\beta_2}\right|_{\beta_1=\beta_2=\beta_0}. \tag{62}$$

Minimization of the above quantity with respect to λ is straightforward, and we get

- if $\Psi(\beta_0) < 0$ then $\lambda = \frac{1}{2}$: the propagation is symmetric,
- if $\Psi(\beta_0) > 0$ then $\lambda = 0$ or $\lambda = 1$: the propagation is asymmetric.

As an illustration of the above discussion, we consider the case of a hard inclusion (see section 3.3), with $\beta_0 = 30°$. The matrix is subjected to a uniaxial remote stress σ^∞_{xx}, and the energy release rate G_1 can be expressed as follows:

$$G_i = (\sigma^\infty_{xx})^2 a\hat{G}_i(\beta_1,\beta_2). \tag{63}$$

Similarly,

$$\Psi(\beta_0) = (\sigma^\infty_{xx})^2 a\hat{\Psi}(\beta_0) \quad\text{with}\quad \hat{\Psi}(\beta_0) = \left.\frac{\partial\hat{G}_1}{\partial\beta_1}\right|_{\beta_1=\beta_2=\beta_0} - \left.\frac{\partial\hat{G}_1}{\partial\beta_2}\right|_{\beta_1=\beta_2=\beta_0} \tag{64}$$

We found numerically that in this case $\hat{\Psi}(\beta_0) = 0.00176 > 0$. Therefore, propagation is asymmetric. It should be noted that despite our thorough numerical investigations, we were not able to produce a case for which symmetric propagation would occur. This might be related to assumption 4, which might be an over-simplifcation (Hutchinson and Suo, 1991).

To close this discussion, it should be mentioned that this analysis is restricted to the onset of the propagation of interfacial cracks. In order to investigate the full equilibrium path beyond the critical load, we would need to assess wether propagation is stable or unstable. This again requires a more realistic propagation criterion, since we observed that Assumption 4 (G_c = const.) tends to favor unstable propagation.

5. Conclusion

The solution to the linear elastic equilibrium of a partially bonded, circular inclusion embedded in a homogeneous matrix and subjected to a uniform stress at infinity was investigated by means of the method of complex potentials (Muskhelishvili, 1953). The analysis was simplified by considering two coaxial cracks, albeit with different lengths. These potentials are then used to determine the stress intensity factors and the energy release rate at the crack tips.

The solution obtained in this paper extends those previously established by Perlman and Sih (1967); Toya (1974); Prasad and Simha (2003) (single crack) and Prasad and Simha (2002) (two coaxial cracks of equal lengths).

Starting from an initial configuration where the two cracks have equal length, the energy criterion of linear elastic fracture mechanics is then used to analyse the propagation of cracks under a remote loading that is symmetric. It is shown that one-sided crack growth is sometimes more favorable than symmetric crack growth.

The solution presented here is the basic building block of micromechanical damage models taking into account partial debonding of the inclusions. This will be investigated in future works. Another interesting perspective would be to investigate crack propagation with a more realistic criterion (see, e.g., Hutchinson and Suo, 1991). Finally, we would like to combine the present analysis of the crack propagation to the analysis of the crack initiation that was performed by Mantič (2009) and García et al. (2015). In the latter reference, using the coupled stress and energy criterion of Leguillon (2002), the authors conclude that asymmetric, rather than symmetric crack nucleation is often to be expected. They attribute the differences with previous studies (Kushch et al., 2011a,b; Bouhala et al., 2013; Carpinteri et al., 2005) to the "smoothness" of the cohesive zone models that have been used. This point ought to be investigated more thoroughly in future studies.

Acknowledgements

This work has benefited from a French government grant managed by ANR within the frame of the national program Investments for the Future ANR-11-LABX-022-01.

Bouhala, L., Makradi, A., Belouettar, S., Kiefer-Kamal, H., Fréres, P., 2013. Modelling of failure in long fibres reinforced composites by x-fem and cohesive zone model. Composites Part B: Engineering 55, 352–361.

Carpinteri, A., Paggi, M., Zavarise, G., 2005. Snap-back instability in microstructured composites and its connection with superplasticity. Strength, Fracture and Complexity 3 (2-4), 61–72.

Erdogan, F., Sih, G., 1963. On the crack extension in plates under plane loading and transverse shear. Journal of basic engineering 85 (4), 519–525.

Gager, J., 2010. Numerical simulations of interface cracks in glued die-attach semiconductor devices. Ph.D. thesis, TU Wien.

García, I., Mantič, V., Graciani, E., 2015. Debonding at the fibre–matrix interface under remote transverse tension. one debond or two symmetric debonds? European Journal of Mechanics-A/Solids 53, 75–88.

Griffith, A. A., 1921. The phenomena of rupture and flow in solids. Philosophical transactions of the royal society of london. Series A, containing papers of a mathematical or physical character 221, 163–198.

Hasebe, N., Okumura, M., Nakamura, T., 1986. Stress analysis of a debonding and a crack around a circular rigid inclusion. International Journal of Fracture 32 (3), 169–183.

Hasebe, N., Yamamoto, Y., 2014. Competition of crack and debonding at the interface of a circular rigid inclusion under uniform loading. Engineering Fracture Mechanics 119, 148–163.

Hasebe, N., Yamamoto, Y., 2015. A crack initiation and two debondings development at the interface of a circular rigid inclusion under uniform loading. International Journal of Damage Mechanics 24 (7), 965–982.

Hutchinson, J. W., Suo, Z., 1991. Mixed mode cracking in layered materials. In: Advances in applied mechanics. Vol. 29. Elsevier, pp. 63–191.

Irwin, G. R., 1957. Analysis of stresses and strains near the end of a crack traversing a plate. Journal of applied mechanics 24 (3), 361–364.

Kushch, V., Shmegera, S., Brøndsted, P., Mishnaevsky, L., 2011a. Numerical simulation of progressive debonding in fiber reinforced composite under transverse loading. International Journal of Engineering Science 49 (1), 17–29.

Kushch, V., Shmegera, S., Mishnaevsky Jr, L., 2010. Elastic interaction of partially debonded circular inclusions. I. Theoretical solution. International Journal of Solids and Structures 47 (14-15), 1961–1971.

Kushch, V. I., Shmegera, S. V., Mishnaevsky, L., 2011b. Explicit modeling the progressive interface damage in fibrous composite: Analytical vs. numerical approach. Composites Science and Technology 71 (7), 989–997.

Leguillon, D., 2002. Strength or toughness? a criterion for crack onset at a notch. European Journal of Mechanics-A/Solids 21 (1), 61–72.

Malyshev, B., Salganik, R., 1965. The strength of adhesive joints using the theory of cracks. International Journal of Fracture 1 (2), 114–128.

Mantič, V., 2009. Interface crack onset at a circular cylindrical inclusion under a remote transverse tension. application of a coupled stress and energy criterion. International journal of Solids and Structures 46 (6), 1287–1304.

Milne-Thomson, L. M., 1968. Plane elastic systems. Vol. 6. Springer.

Muskhelishvili, N. I., 1953. Some basic problems of the mathematical theory of elasticity. Noordhoff, Groningen, The Netherlands.

Perlman, A., Sih, G., 1967. Elastostatic problems of curvilinear cracks in bonded dissimilar materials. International Journal of Engineering Science 5 (11), 845–867.

Pouya, A., 2015. A finite element method for modeling coupled flow and deformation in porous fractured media. International Journal for Numerical and Analytical Methods in Geomechanics 39 (16), 1836–1852.

Prasad, P., Simha, K., 2002. Interactions of interfacial arc cracks. International Journal of Fracture 117 (1), 39–62.

Prasad, P., Simha, K., 2003. Interface crack around circular inclusion: Sif, kinking, debonding energetics. Engineering Fracture Mechanics 70 (2), 285–307.

Rice, J., 1988. Elastic fracture mechanics concepts for interfacial cracks. J. Appl. Mech.(Trans. ASME) 55 (1), 98–103.

Ryoji, Y., Sang-Bong, C., 1989. Efficient boundary element analysis of stress intensity factors for interface cracks in dissimilar materials. Engineering Fracture Mechanics 34 (1), 179–188.

Sun, C., Jin, Z., 2012. Fracture mechanics. Academic Press, Boston.

Sun, C., Qian, W., 1997. The use of finite extension strain energy release rates in fracture of interfacial cracks. International Journal of Solids and Structures 34 (20), 2595 – 2609.

Sun, C. T., Jih, C., 1987. On strain energy release rates for interfacial cracks in bi-material media. Engineering Fracture Mechanics 28 (1), 13–20.

Theotokoglou, E., Theotokoglou, E., 2002. The interface crack along a circular inclusion interacting with a crack in the infinite matrix. International journal of fracture 116 (1), 1–23.

Toya, M., 1974. A crack along the interface of a circular inclusion embedded in an infinite solid. Journal of the Mechanics and Physics of Solids 22 (5), 325–348.

Williams, M., 1959. The stresses around a fault or crack in dissimilar media. Bulletin of the seismological society of America 49 (2), 199–204.